

Research Article

Sensor Fault Tolerant Control of a Fast Steering Mirror System Using Adaptive PI-Based Sliding Mode Observer and Hardware Redundancy

Hongju Wang,^{1,2,3} Qiliang Bao,^{1,2} Wenshu Yang,² Zidong Liu,^{1,2} and Jing Tian^{1,2}

¹Key Laboratory of Optical Engineering, Chinese Academy of Sciences, Mailbox 350, Chengdu 610209, China

²Institute of Optics and Electronics, Chinese Academy of Sciences, Mailbox 350, Chengdu 610209, China

³University of Chinese Academy of Sciences, Beijing 100191, China

Correspondence should be addressed to Hongju Wang; ioe_whj@163.com

Received 24 June 2014; Accepted 1 September 2014

Academic Editor: Ke Zhang

Copyright © 2015 Hongju Wang et al. This is an open access article distributed under the Creative Commons Attribution License, which permits unrestricted use, distribution, and reproduction in any medium, provided the original work is properly cited.

The aim of this paper is to present a sensor fault-tolerant control (FTC) scheme for a two-axis fast steering mirror (FSM) system with minimum power consumption and without changing the controller structure. In this paper, an adaptive PI-based sliding mode observer (APISMO) is adopted firstly to estimate the fault signal, which does not require any prior knowledge of the fault. The estimation is then used by the fault isolation logic to identify the fault. The redundant sensor would be powered up to replace the faulty one when faults occur. During the backup sensor booting up, for maintaining the normal performance of the closed-loop system approximately, a fault-free estimation of the position provided by the APISMO is used as feedback signal. Experimental studies on a prototype system show that the proposed APISMO can effectively reconstruct the fault signals even when the two primary position sensors are faulty simultaneously. Meanwhile, the effectiveness and performance of the proposed scheme have been verified.

1. Introduction

The fast steering mirror (FSM) system is popularly applied in situations that require a precision positioning, such as space telescopes, adaptive optics, and free-space optical (FSO) communications [1–3]. In most of the applications, the FSM is adopted to steer the optical beam precisely. Extensive researches have been carried out to improve the closed-loop performance of FSM [4–6]. Most of the control strategies depend on reliable sensor measurements. However, these sensors are usually affected by failures such as offset, drift, and disconnection, which would obviously result in overall performance deterioration. Therefore, it is desirable to develop a sensor FTC scheme for FSM.

To maintain a high level of reliability, the hardware redundancy-based technique has been widely used by the FSM system designed for space application [2, 3, 7]. Because of mass and power constraints, it is still a challenge to design a FTC scheme that provides required reliability with

minimum hardware redundancy. In addition, most sensors and actuators have moving parts and life limited components. Another challenge is determining whether the redundant sensors could be kept unpowered and activated only when necessary [8].

Many approaches have been proposed to overcome the aforementioned problems [9–13]. Among them, the analytical redundancy method is particularly effective. By developing mathematical model of the system, analytical redundancy approach could generate estimations of the measurable or unmeasured variables. The estimations can be used to replace the redundant hardware sensors or design fault diagnosis (FD) scheme. To design an active FTC scheme, the first step is to implement a FD scheme to monitor the system and isolate the fault. Adaptive observer-based FD and sliding mode observer-based FD are two extensively studied methods [14–19]. When the faulty physical sensor has been detected and isolated, its measurement would be replaced by the

estimation, which is the so-called virtual sensor. A fault reconstruction scheme using sliding mode observer is also given in [18, 20, 21]. FTC scheme in terms of correcting the measured output signals using reconstructed fault signals is considered in [17, 21, 22]. However, neither the virtual sensor nor measurement corrected by reconstructed signal is as accurate as the fault-free physical sensor. FTC schemes with only analytical redundancy would have a degraded performance in case of sensor faults. That is one of the reasons why the advanced analytical redundancy-based FTC methods have not been really accepted by the aerospace end-users [23].

This paper develops a FTC scheme for the FSM by combining the sliding mode observer-based method and hardware redundancy. The proposed method could improve the performance of the FSM system with faulty sensors and make it more acceptable to the end-users. A FSM model is firstly developed. Based on the FSM model, an APISMO building on the work [20] is proposed to reconstruct the sensor faults faithfully. Different from the observer used in [20], the discontinuous switching function used in conventional SMO is replaced with an adaptive PI function [24, 25]. The proposed APISMO does not require any prior knowledge of the faults. The reconstructed information is then used by the fault isolation logic to identify the fault and power up the redundant sensors. The redundant sensors are kept unpowered in fault-free case, which reduces the power consumption. However, a period of time is required to activate the backup sensors, during which the measurement of the backup is uncertain. In this proposed scheme, a fault-free estimation of the position provided by the APISMO is used as feedback signal to maintain the desired performance during the cold backup booting-up.

From an industrial perspective, the proposed scheme here is easier to be implemented than the conventional SMO. It does not need to know the bounds of the faults and could maintain the desired fault-free performance in failure case. Compared with the FSM using triple modular redundancy (TMR), the proposed scheme could maintain a higher level of reliability with only dual redundancy. Moreover, the redundant sensors are unpowered in fault-free case. Furthermore, the controller structure does not need to be changed in failure case.

This paper is organized as follows. In Section 2, the considered FSM system and its dynamics model are described. Section 3 presents the fault estimation method based on the proposed APISMO. Section 4 introduces the proposed FTC scheme with the hardware redundancy and the fault isolation logic. Experimental results of the proposed scheme are given in Section 5, followed by some concluding remarks in Section 6.

2. FSM Model

2.1. System Description. A FSM is generally defined as a mirror mounted to a flexure support system and driven by actuators [6]. The prototype of a two-axis FSM is shown in Figure 1. It consists of six important components: a mirror assembly, a flexure suspension, a mirror base, voice coil

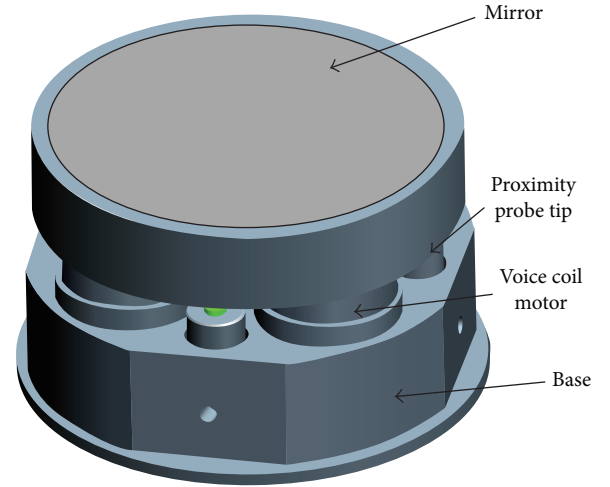


FIGURE 1: Prototype of the fast steering mirror.

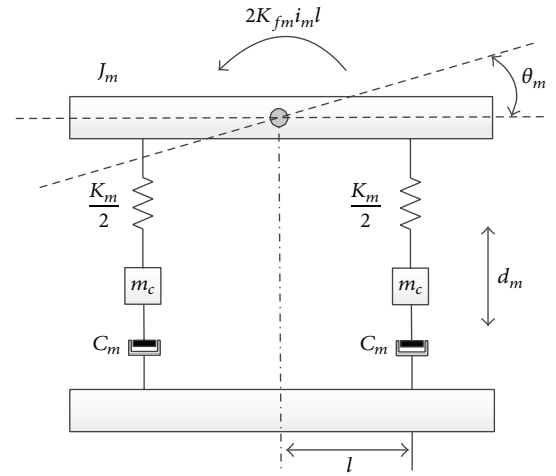


FIGURE 2: Schematic diagram of FSM in single axis.

motors (VCMs), proximity sensors, and drive electronics. Two voice-coils operating in push-pull manner are fixed on the back of the mirror, rotating the mirror about the axis that bisects them. Therefore, two actuator pairs are used to produce two orthogonal rotations (θ_x, θ_y) . A flexure suspension system is used to support the mirror carrier which holds the mirror. This system allows free rotation about orthogonal x - and y -axes while constraining piston, side-to-side, and rotation about the normal axis [26].

2.2. Dynamics Model. To establish the dynamics model of a two-axis FSM, it is assumed that the motions rotating about the two orthogonal x - and y -axes are decoupling with each other. The x -axis motion and y -axis motion follow the same working principle. The motions can be equivalently represented by a sketch of spring-mass-dashpot system shown in Figure 2 [27]. The dynamics model of the two-axis FSM can be given as

$$(J_m + 2m_c l^2) \ddot{\theta}_m + 2C_m l^2 \dot{\theta}_m + K_m \theta_m = 2K_{fm} i_m l, \quad (1)$$

where $m = x$ or y ; here J_m is moment of inertia of the mirror rotating about x - or y -axis. Parameters m_c , l , θ_m , C_m , and K_m represent mass of the voice-coil, the distance between actuator and the axis, deflection angle, damping coefficient, and spring constant, respectively; K_{fm} is the force constant and i_m denotes the driving current.

The actuator driver receives voltage commands from the controller and converts them to driving current. Its dynamical characteristics satisfy Kirchoff's voltage law

$$U_m = L_m \frac{di_m}{dt} + i_m R_m + k_b \dot{d}_m, \quad (2)$$

where U_m is the voltage and parameters L_m , R_m , k_b , and d_m represent the coil inductance, coil resistance, back electromotive force constant, and the displacement of the coil.

The deflection angle is generally very small; thus the displacement of the coil d_m can be approximated as a function of the deflection angle θ_m ; that is, $d_m = l\theta_m$. Substituting (2) into (1) yields

$$\begin{aligned} & L_m (J_m + 2m_c l^2) \ddot{\theta}_m + [2L_m C_m l^2 + R_m (J_m + 2m_c l^2)] \\ & \times \dot{\theta}_m + (2k_{fx} k_b l^2 + L_m k_m + 2R_m C_m l^2) \\ & \times \theta_m + R_m k_m \theta_m = 2k_{fm} l U_m. \end{aligned} \quad (3)$$

Rewrite (3) in a state-space form as

$$\dot{X}(t) = AX(t) + Bu(t), \quad (4)$$

$$X(t) = [x_1(t), x_2(t), x_3(t), y_1(t), y_2(t), y_3(t)]^T = [\theta_x(t), \dot{\theta}_x(t), \ddot{\theta}_x(t), \theta_y(t), \dot{\theta}_y(t), \ddot{\theta}_y(t)]^T,$$

$$A = \begin{bmatrix} 0 & 1 & 0 & & & \\ 0 & 0 & 1 & & & \\ \frac{-R_x k_x}{L_x (J_x + 2m_c l^2)} & \frac{2k_{fx} k_b l^2 + L_x k_x + 2R_x C_x l^2}{L_x (J_x + 2m_c l^2)} & \frac{2L_x C_x l^2 + R_x (J_x + 2m_c l^2)}{L_x (J_x + 2m_c l^2)} & & & \\ & & & 0_{3 \times 3} & & \\ & & & & 0 & \\ & & & & 0 & 1 \\ & & & & \frac{-R_y k_y}{L_y (J_y + 2m_c l^2)} & \frac{2k_{fy} k_b l^2 + L_y k_y + 2R_y C_y l^2}{L_y (J_y + 2m_c l^2)} \\ & & & & & \frac{2L_y C_y l^2 + R_y (J_y + 2m_c l^2)}{L_y (J_y + 2m_c l^2)} \end{bmatrix},$$

$$B = \begin{bmatrix} 0 & & & & & \\ 0 & & & & & \\ \frac{2k_{fx} l}{L_x (J_x + 2m_c l^2)} & & & & & \\ 0 & & & & & \\ 0 & & & & & \\ 0 & & & & & \\ & & & & \frac{2k_{fy} l}{L_y (J_y + 2m_c l^2)} & \end{bmatrix}. \quad (5)$$

3. APISMO Design and Fault Reconstruction

In order to reconstruct the sensor fault signal, an APISMO based on the dynamics model (4) is proposed in this section. For better understanding, the preliminaries and design of the conventional SMO are introduced firstly.

3.1. Preliminaries. This section introduces the preliminaries for using a SMO to reconstruct sensor faults. Consider the following linear system affected by sensor faults:

$$\dot{X}(t) = AX(t) + Bu(t), \quad (6)$$

$$Y(t) = CX(t) + Ff_i(t), \quad (7)$$

where $A \in R^{n \times n}$, $B \in R^{n \times m}$, $C \in R^{p \times n}$, and $F \in R^{p \times r}$. The matrices C and F are full row and column rank, respectively.

The function $f_i(t)$ is unknown but bounded sensor fault signal.

An effective way to reconstruct the sensor fault $f_i(t)$ is introducing a filter first [18, 22]. Define a new state Z_f , satisfying

$$\dot{Z}_f(t) = -A_f Z_f(t) + A_f Y(t), \quad (8)$$

where $-A_f \in R^{p \times p}$ is a stable matrix. Substituting (7) into (8) yields

$$\dot{Z}_f(t) = -A_f Z_f(t) + A_f CX(t) + A_f Ff_i(t). \quad (9)$$

By combining (6) and (9) and defining new states $X_a = \text{col}(X(t), Z_f(t))$, an augmented system can be given as

$$\begin{aligned} \underbrace{\begin{bmatrix} \dot{X}(t) \\ \dot{Z}_f(t) \end{bmatrix}}_{\dot{X}_a} &= \underbrace{\begin{bmatrix} A & 0 \\ A_f C & -A_f \end{bmatrix}}_{A_a} \begin{bmatrix} X(t) \\ Z_f(t) \end{bmatrix} + \underbrace{\begin{bmatrix} B \\ 0 \end{bmatrix}}_{B_a} u(t) \\ &+ \underbrace{\begin{bmatrix} 0 \\ A_f F \end{bmatrix}}_{F_a} f_i(t), \end{aligned} \quad (10)$$

$$Z_f(t) = \underbrace{\begin{bmatrix} 0 & I_p \\ C_a \end{bmatrix}}_{C_a} \begin{bmatrix} X(t) \\ Z_f(t) \end{bmatrix}.$$

3.2. Conventional Sliding Mode Observer for Fault Reconstruction. Considering the new dynamical system in (10), the conventional SMO is constructed as [20]

$$\dot{\hat{X}}_a = A_a \hat{X}_a + B_a u(t) - G_l e_y(t) + G_n v. \quad (11)$$

In (11), the discontinuous term v is

$$v = \begin{cases} -\rho \|F_2\| \frac{P_0 e_y}{\|P_0 e_y\|} & \text{if } e_y \neq 0, \\ 0 & \text{otherwise,} \end{cases} \quad (12)$$

where $e_y = C_a \hat{X}_a - Z_f$ is the output estimation error and P_0 is a symmetric positive definite (s.p.d.) matrix. The matrices G_l, G_n, F_2 , and P_0 will be described later. The scalar ρ must be upper bound on the faults.

It has been proven in [20] that a SMO of the form (11) and (12) which is not affected by the fault $f_i(t)$ exists if and only if

$$(A1) \text{ rank}(C_a F_a) = r,$$

$$(A2) \text{ invariant zeros of } (A_a, F_a, C_a) \text{ are stable.}$$

Then if the assumptions (A1) and (A2) are satisfied [20], there exists a change of coordinates $X_a = T_a X_a$, in which the new triple $(\bar{A}_a, \bar{F}_a, \bar{C}_a)$ has the following structure:

$$\begin{aligned} \bar{A}_a &= \begin{bmatrix} A_{11} & A_{12} \\ A_{21} & A_{22} \end{bmatrix}, & \bar{F}_a &= \begin{bmatrix} 0 \\ F_2 \end{bmatrix}, \\ \bar{C}_a &= [0 \quad I_p], \end{aligned} \quad (13)$$

where $A_{11} \in R^{n \times n}$ is a stable matrix, $A_{12} \in R^{n \times p}$, $A_{21} \in R^{p \times n}$, $A_{22} \in R^{p \times p}$, $F_2 \in R^{p \times r}$.

Considering the structure (13), the observer gains in (11) can be obtained as

$$G_l = T_a^{-1} \begin{bmatrix} A_{12} \\ A_{22} - A_s \end{bmatrix}, \quad G_n = T_a^{-1} \begin{bmatrix} 0 \\ I_p \end{bmatrix}, \quad (14)$$

where A_s is a stable matrix which is chosen to make $(A_a - G_l C_a)$ stable. The matrix P_0 is the unique solution to the Lyapunov equation of A_s [20].

On condition that the assumptions (A1) and (A2) are satisfied, it could be shown that an ideal sliding motion takes place on the surface (15) in finite time:

$$S_0 = \{e : C_a e = 0\}. \quad (15)$$

During the ideal sliding motion, $e_y = 0$ and $\dot{e}_y = 0$, the discontinuous signal v will take on average a value to compensate for the fault signal while maintaining a sliding motion [20, 22]. The average quantity can be computed online as

$$v_\delta = -\rho \|F_2\| \frac{P_0 e_y}{\|P_0 e_y\| + \delta}, \quad (16)$$

where δ is a small positive scalar.

Consequently, a fault reconstruction signal is

$$\hat{f}_i(t) \approx -\rho \|F_2\| (F_2^T F_2)^{-1} F_2^T \frac{P_0 e_y}{\|P_0 e_y\| + \delta}. \quad (17)$$

For details, see [20, 22].

In fact, design of the conventional SMO needs to know the upper bounds of the faults in advance. However, in practice, these bounds are difficult to obtain. Many literatures take an approximate upper estimation of the faults signal as scalar ρ . However, some additional dynamics would be introduced by this method. Moreover, if the fault is larger than the scalar ρ , the conventional method cannot reconstruct the fault properly.

3.3. APISMO Design and Fault Reconstruction. To overcome the problems associated with the conventional SMO, an APISMO building on the conventional SMO is proposed by replacing the saturation function in (16) with a continuous term determined by an adaptive PI algorithm. The proposed APISMO has the same structure with the observer in Section 3.2, except that the saturation function is replaced with an adaptive PI function.

The proposed PI function in APISMO takes the sliding surface function S_0 as the input. The PI function is defined as

$$v_{PI} = k_p e_y(t) + k_i \int e_y(t) dt, \quad (18)$$

where the sliding surface function $C_a e = e_y$ and k_p and k_i are the proportional gain and integral gain.

Substitute (18) into (11) and take a change of coordinates $\bar{X} = [\hat{x}_1 \quad \hat{x}_2]^T = T_a \hat{X}_a$. In the new coordinate system, the APISMO can be defined as

$$\begin{aligned} \dot{\hat{x}}_1(t) &= A_{11} \hat{x}_1(t) + A_{12} \hat{x}_2(t) + B_1 u(t) - A_{12} e_y(t), \\ \dot{\hat{x}}_2(t) &= A_{21} \hat{x}_1(t) + A_{22} \hat{x}_2(t) + B_2 u(t) \\ &- (A_{22} - A_s) e_y(t) + v_{PI}, \end{aligned} \quad (19)$$

$$\hat{Y}(t) = \hat{x}_2(t).$$

In the new coordinate system, defining new states $X = [x_1, x_2]^T = T_a X_a$, then the dynamical system given by (10) has a structure as

$$\begin{aligned} \begin{bmatrix} \dot{x}_1(t) \\ \dot{x}_2(t) \end{bmatrix} &= \begin{bmatrix} A_{11} & A_{12} \\ A_{21} & A_{22} \end{bmatrix} \begin{bmatrix} x_1(t) \\ x_2(t) \end{bmatrix} + \begin{bmatrix} B_1 \\ B_2 \end{bmatrix} u(t) + \begin{bmatrix} 0 \\ F_2 \end{bmatrix} f_i(t), \\ Y(t) &= [0 \quad I_p] \begin{bmatrix} x_1(t) \\ x_2(t) \end{bmatrix}. \end{aligned} \quad (20)$$

Define the state vector of the estimation error as

$$E = [e_1 \ e_2]^T = \widehat{X} - X = [\widehat{x}_1 - x_1 \ \widehat{x}_2 - x_2]^T. \quad (21)$$

By taking the first derivative of (21) and substituting (19) and (20), we have

$$\dot{e}_1(t) = A_{11}e_1(t), \quad (22)$$

$$\begin{aligned} \dot{e}_y(t) = & A_{21}e_1(t) + A_s e_y(t) + k_p e_y(t) \\ & + k_i \int e_y(t) dt - F_2 f_i(t), \end{aligned} \quad (23)$$

where $e_y(t) = e_2(t)$ in this situation.

For reconstructing sensor faults properly, the sliding surface S_0 in (15) must be reachable. The reachability of the sliding surface S_0 is determined by the proportional gain k_p and integral gain k_i according to the following theorem.

Theorem 1. *Under the assumptions (A1) and (A2), for the error system given by (22) and (23), the sliding mode surface S_0 in (15) is asymptotically reachable, that is, $e_y \rightarrow 0$ as $t \rightarrow \infty$, if and only if $k_i \neq 0$ and the roots of*

$$s^2 - A_s s - k_p s - k_i = 0 \quad (24)$$

have negative real parts, where s is the Laplace transform operator.

Proof. Considering that most aerospace systems have self-testing at startup, it is reasonable to assume that there exist no faults at initial time. Therefore, $f_i(t)$ has zero initial value and $e_1(t)$ could have a nonzero initial value, then decomposing $e_1(t)$ as

$$e_1(t) = e_{10}(0) + e_{11}(t), \quad (25)$$

where $e_{10}(0) \equiv e_1(0)$ is the initial value of $e_1(t)$ and $e_{11}(t)$ is the other part of $e_1(t)$ and has zero initial value.

Substituting (25) into (23) yields

$$\begin{aligned} \dot{e}_y(t) = & A_{21}e_{10}(0) + A_{21}e_{11}(t) + A_s e_y(t) + k_p e_y(t) \\ & + k_i \int e_y(t) dt - F_2 f_i(t). \end{aligned} \quad (26)$$

The system defined by (26) can be regarded as a linear system with three inputs, that is, $e_{10}(0)$, $e_{11}(t)$, and $f_i(t)$. Then this linear system could be decomposed into three subsystems. Each subsystem takes one of the inputs, that is, $e_{10}(0)$, $e_{11}(t)$, and $f_i(t)$, as its input while its output being a part of $e_y(t)$, that is, $e_{yn}(t)$, $n = 1, 2, 3$. For the sliding mode surface S_0 in (15) to be asymptotically reachable, that is, $e_y \rightarrow 0$ as $t \rightarrow \infty$, the error system (26) must be stable. That is, all the three subsystems must be stable. Following that, each subsystem is examined.

The first subsystem has $e_{11}(t)$ as input and $e_{y1}(t)$ as output. The transfer function can be obtained as

$$\frac{e_{y1}(s)}{e_{11}(s)} = \frac{sA_{21}}{s^2 - A_s s - k_p s - k_i}. \quad (27)$$

It can be seen that the first subsystem (27) is asymptotically stable if and only if the roots of (24) have negative real parts and $k_i \neq 0$.

According to the assumptions (A1) and (A2), the matrix A_{11} is stable, and then $e_{11}(\infty) \rightarrow 0$. Applying the final value theorem to $e_{y1}(s)$ yields

$$e_{y1}(\infty) = \lim_{s \rightarrow 0} \frac{s * sA_{21}e_{11}(s)}{s^2 - A_s s - k_p s - k_i} = 0. \quad (28)$$

It is easy to find that the remaining two subsystems are asymptotically stable if and only if the roots of (24) have negative real parts and $k_i \neq 0$ and

$$e_{y2}(\infty) = 0, \quad e_{y3}(\infty) = 0. \quad (29)$$

Therefore, the error system given by (23) or (26) is asymptotically stable if and only if the roots of (24) have negative real parts and $k_i \neq 0$. Given the stability condition is satisfied, then

$$e_y(\infty) = e_{y1}(\infty) + e_{y2}(\infty) + e_{y3}(\infty) = 0. \quad (30)$$

That is, the sliding mode surface S_0 in (15) is asymptotically reachable.

According to Theorem 1, for a given proportional gain k_p of the APISMO, there exists a nonzero integral gain k_i^* such that the sliding surface (15) is asymptotically reachable; that is, with $v_{PI} = k_p e_y(t) + k_i^* \int e_y(t) dt$, the condition $\dot{S}_0 S_0 < -\eta |S_0|$ is satisfied, where η is a positive scalar [25]. \square

Defining the integral gain estimation error as (31) and a Lyapunov function as (32)

$$\tilde{k}_i = k_i^* - k_i, \quad (31)$$

$$V = \frac{1}{2} (s_0^2 + \alpha \tilde{k}_i^2), \quad (32)$$

where α is a positive constant. Taking the first derivative of V yields

$$\dot{V} = s_0 \dot{s}_0 + \alpha \tilde{k}_i \dot{\tilde{k}}_i. \quad (33)$$

Substituting (23) and (31) into (33) results in

$$\begin{aligned} \dot{V} = & e_y(t) \left[A_{21}e_1(t) + A_s e_y(t) + k_p e_y(t) \right. \\ & \left. + k_i^* \int e_y(t) dt - F_2 f_i(t) \right] \\ & - \tilde{k}_i e_y(t) \int e_y(t) dt + \alpha \tilde{k}_i \dot{\tilde{k}}_i \\ \leq & -\eta |s_0| - \tilde{k} \left[e_y(t) \int e_y(t) dt - \alpha \dot{\tilde{k}}_i \right]. \end{aligned} \quad (34)$$

Thus the adaptive law for k_i can be obtained as

$$\dot{\tilde{k}}_i = \frac{1}{\alpha} e_y(t) \int e_y(t) dt. \quad (35)$$

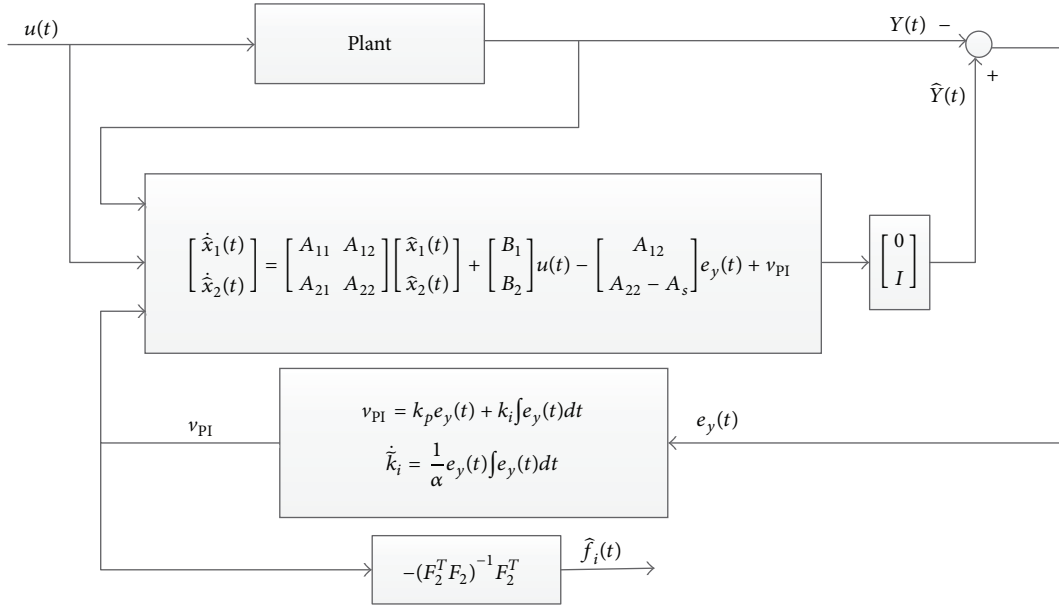


FIGURE 3: Schematic diagram of the proposed APISMO implementation.

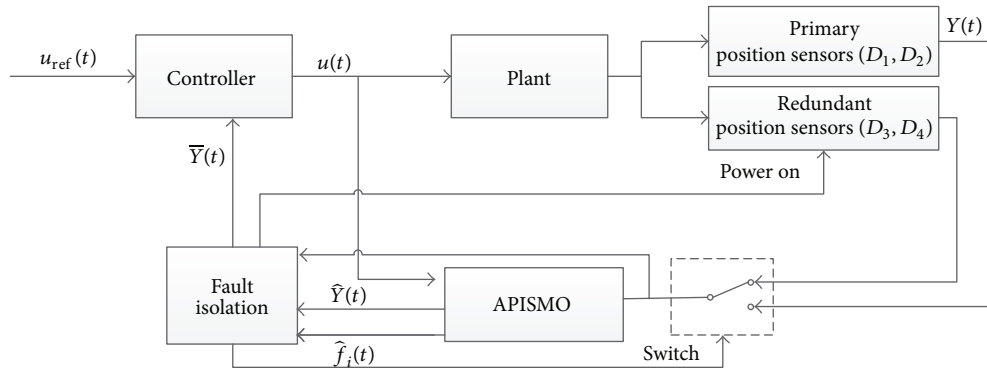


FIGURE 4: Schematic diagram of the proposed FTC scheme.

Finally, the sensor fault can be reconstructed properly by the APISMO as

$$\begin{aligned} \hat{f}_i(t) &\approx -(F_2^T F_2)^{-1} F_2^T v_{PI} \\ &\approx -(F_2^T F_2)^{-1} F_2^T \left[k_p e_y(t) + k_i \int e_y(t) dt \right], \end{aligned} \quad (36)$$

where the adaptive law for k_i is

$$\dot{\hat{k}}_i = \frac{1}{\alpha} e_y(t) \int e_y(t) dt = \gamma e_y(t) \int e_y(t) dt, \quad (37)$$

where $\gamma = 1/\alpha$.

For better understanding, a schematic representation of the proposed APISMO and fault reconstruction is shown in Figure 3.

4. Fault-Tolerant Control Design

In this section, to improve the performance of the system with only SMO-based FTC scheme, a FTC scheme for FSM is

presented by combining the proposed APISMO and the hardware redundancy. Position sensors installed with dual redundancy are used in the proposed FTC scheme. Figure 4 shows the block diagram of the proposed FTC scheme.

4.1. Redundancy Design. At the design stage of the FSM, the sensors were installed with dual redundancy. The redundant sensors are functionally identical to the primary sensors by placing them at symmetrical locations of the primary ones. The placements of the sensors are illustrated in Figure 5. D_1 and D_2 denote the primary sensor probes; D_3 and D_4 are redundant ones. Four proximity probe tips are placed at 90 degrees from each other and 45 degrees from each VCM. The distances between each probe tip and the x - and y -axes are equal, which is denoted by l .

The proximity sensor system provides an output voltage that is directly proportional to the distance between probe tip and the moving mirror. Since deflection angle of the mirror is generally very small, the output voltage of the proximity

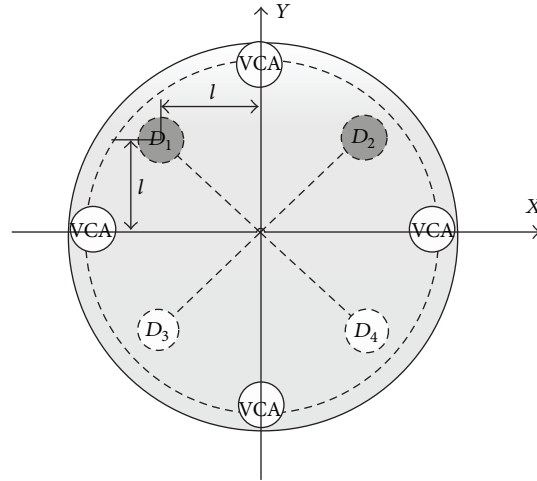


FIGURE 5: The placement of the sensors.

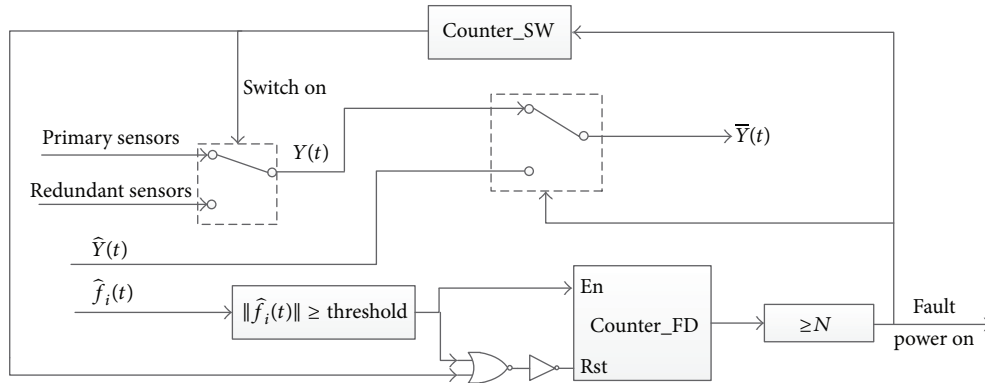


FIGURE 6: Schematic diagram of the fault isolation logic.

sensor system can be used to approximate the deflection angle by the following equation:

$$\begin{aligned} D_1 &= kl(\theta_x + \theta_y), & D_4 &= -kl(\theta_x + \theta_y), \\ D_2 &= kl(\theta_x - \theta_y), & D_3 &= -kl(\theta_x - \theta_y), \end{aligned} \quad (38)$$

where $D_1, D_2, D_3,$ and D_4 are the output voltages of the four sensors and k is the proportional scalar of the sensor.

4.2. Fault Isolation Logic. In order to keep the feedback signal used by controller free from sensor faults, fault isolation logic shown in Figure 6 is adopted. In fault-free case, the reconstructed fault signal in (36) is approximately zero. The measurements of the primary sensors are used as feedback signals. If the reconstructed signal exceeds a threshold, the counter Counter_FD begins to work simultaneously, which is used to obtain information on how long a threshold has been crossed. If the value of the counter is greater than or equal to N counter-steps, the measurement D_i is identified to be faulty; a signal would be sent out to power on the redundancy.

Since a period of time is required to activate the cold backup sensor, during the cold backup booting up, the measurement of the backup is uncertain. A fault-free estimation

of the position provided by the APISMO is used as feedback signal to maintain the desired performance. The counter Counter_SW is used to calculate the activation time and send out switch signal. After the backup is activated, the faulty sensor is replaced by the redundant one and the measurement of the redundant sensor is used as feedback signal.

5. Experimental Results

In this section, to validate the effectiveness of the proposed scheme, a series of experimental studies were conducted on a prototype of the FSM.

5.1. Experimental Setup. The experimental setup of a FSM system is depicted in Figure 7. The tilt of the mirror relative to the fixed base is measured by four proximity sensors placed as in Figure 5. The proximity sensor system provides a measuring range of 2 mm and an output of 20 V/mm. In addition, an embedded computer MICROSPACE PC/104 (from Digital Logic corp.) equipped with a PC/104 expansion board Diamond-MM-16-AT (from Diamond Systems Corp.) offering 12-bit D/A converter and 16-bit A/D converter is adopted to produce excitation voltage signals and acquire

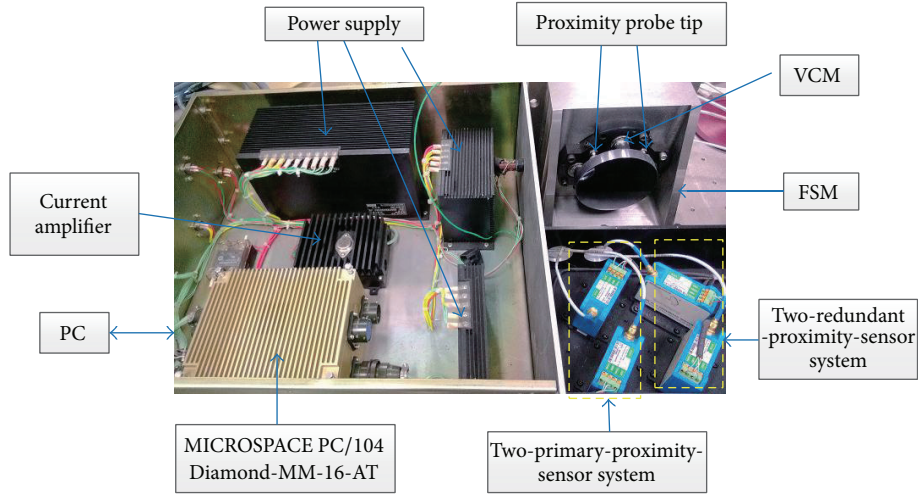


FIGURE 7: Experimental setup of a fast steering mirror system.

the sensor readings. The APISMO, fault isolation logic, and conventional PI control algorithms are developed with MATLAB/Simulink software and downloaded to MICROSPACE PC/104 to realize a real-time fault-tolerant control. The sampling interval used in the experiments is $200 \mu\text{s}$.

5.2. Plant Model Identification. The mathematical model of the FSM can be identified by using a dynamical signal analyzer. The swept-sine waves applied to the actuators have the amplitude of 0.3 V and frequency range of $1\text{--}2000 \text{ Hz}$. The position responses of the steering mirror in two orthogonal directions are recorded using a sampling rate of 5 kHz . With a push-pull pair of actuators driven, the magnitudes of the output displacement in passive axis are 20 dB lower than that in the major axis, which indicates that the two axial motions of the steering mirror are decoupled [28]. Transfer function G_{px} of the plant rotating about x -axis can be identified by using the input-output data sets.

The identified third-order transfer function is

$$G_{px}(s) = \frac{275100}{s^3 + 2861s^2 + 155400s + 1.715 \times 10^8}. \quad (39)$$

In the same way, transfer function G_{py} of the plant rotating about y -axis can be obtained as

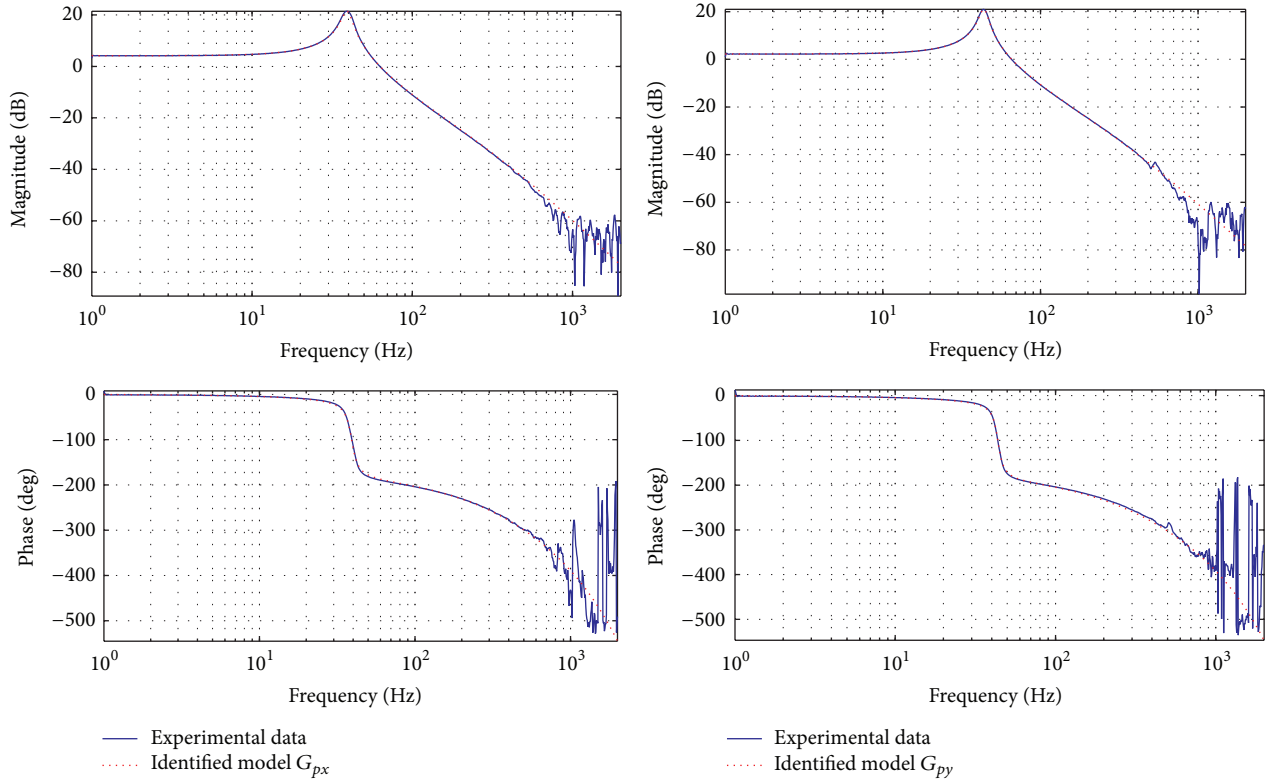
$$G_{py}(s) = \frac{244000}{s^3 + 2543s^2 + 154600s + 1.903 \times 10^8}. \quad (40)$$

The identified models G_{px} in (39) and G_{py} in (40) and the frequency responses of the FSM obtained from the experimental data are shown in Figure 8.

Comparing (3) with the inverse Laplace transform of (39) and (40) yields the system matrix A and input distribution matrix B of the state-space model (4)

$$A = \begin{bmatrix} 0 & 1 & 0 & 0 & 0 & 0 \\ 0 & 0 & 1 & 0 & 0 & 0 \\ -171500000 & -155400 & -2861 & 0 & 0 & 0 \\ 0 & 0 & 0 & 0 & 1 & 0 \\ 0 & 0 & 0 & 0 & 0 & 1 \\ 0 & 0 & 0 & -190300000 & -154600 & -2543 \end{bmatrix},$$

$$B = \begin{bmatrix} 0 & 0 \\ 0 & 0 \\ 275100 & 0 \\ 0 & 0 \\ 0 & 0 \\ 0 & 244000 \end{bmatrix}.$$


 FIGURE 8: Frequency responses of x - and y -axes, respectively.

The fault distribution matrix F in (7) is defined as $F = I_2$. In (38), the scale k of the proximity sensors is 20 V/mm. The distance between each probe tip and the rotation axis l is 5.02 cm. Thus, the output matrix C has the form

$$C = \begin{bmatrix} 1003.94 & 0 & 0 & 1003.94 & 0 & 0 \\ 1003.94 & 0 & 0 & -1003.94 & 0 & 0 \end{bmatrix}. \quad (42)$$

5.3. Reconstruction of Sensor Faults. In this section, the fault reconstruction performance of the proposed APISMO is verified by being compared with that of the conventional SMO. A conventional SMO is designed firstly. The influence of filter matrix A_f on the performance of fault estimation system has been investigated in [29]. Here, the matrix was chosen as $A_f = 1500I_2$. It can be seen that system matrix A given in (41) is stable; therefore, the conditions (A1) and (A2) are satisfied. The design parameters (from (14) and (16)) were chosen as $A_s = -50I_2$ and $\delta = 0.1$. Assuming that the upper bound of the faults is 0.4 mm, the scalar ρ was set as $\rho = 8$. The positive-definite matrix P_0 (from (16)) was selected

by solving the Lyapunov function of A_s . The associated gains in (14) were obtained as

$$G_l = \begin{bmatrix} 0 & 0 & 0 \\ 0 & 0 & 0 \\ 0 & 0 & 0 \\ 0 & 0 & 0 \\ 0 & 0 & 0 \\ -950 & 0 & 0 \\ 0 & -950 & 0 \\ 0 & 0 & -950 \end{bmatrix}, \quad G_n = \begin{bmatrix} 0 & 0 & 0 \\ 0 & 0 & 0 \\ 0 & 0 & 0 \\ 0 & 0 & 0 \\ 0 & 0 & 0 \\ 1 & 0 & 0 \\ 0 & 1 & 0 \\ 0 & 0 & 1 \end{bmatrix}. \quad (43)$$

The associated gains for the APISMO were the same as that in (43). The parameters for the adaptive PI function were chosen as $k_p = 1000I_2$, $k_{i\text{-initial}} = I_2$, and $\gamma = 0.01$.

In the experiments, the two primary sensors were corrupted by the faults illustrated in Figure 9 simultaneously. The system is open-loop system. The value of the fault acting on sensor D_1 is smaller than the scalar ρ , whereas the value of the fault acting on sensor D_2 is larger than the scalar. It is shown in Figure 10 that the proposed APISMO reconstructs the fault faithfully. In comparison, Figure 11 shows the fault signal reconstructed by the conventional SMO. It can be seen from Figures 10(a) and 11(a) that both methods could obtain a very proper reconstruction when the difference between the fault signal and the scalar ρ is not significant. However, as

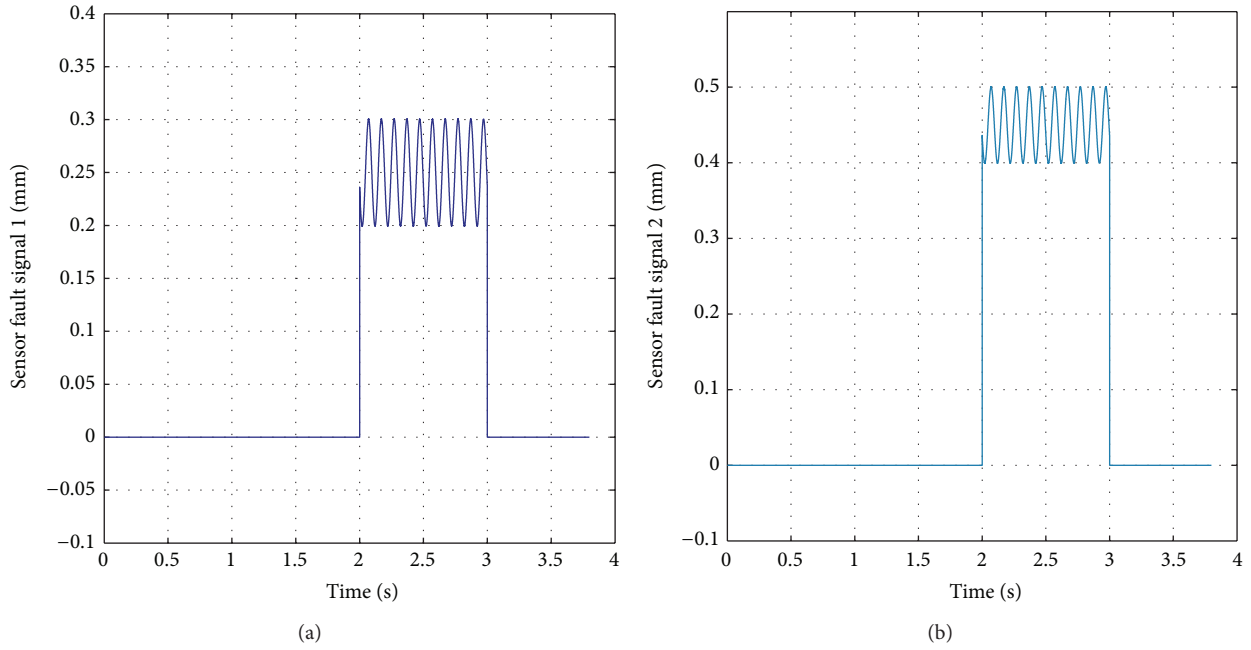


FIGURE 9: (a) Fault acting on sensor D_1 . (b) Fault acting on sensor D_2 .

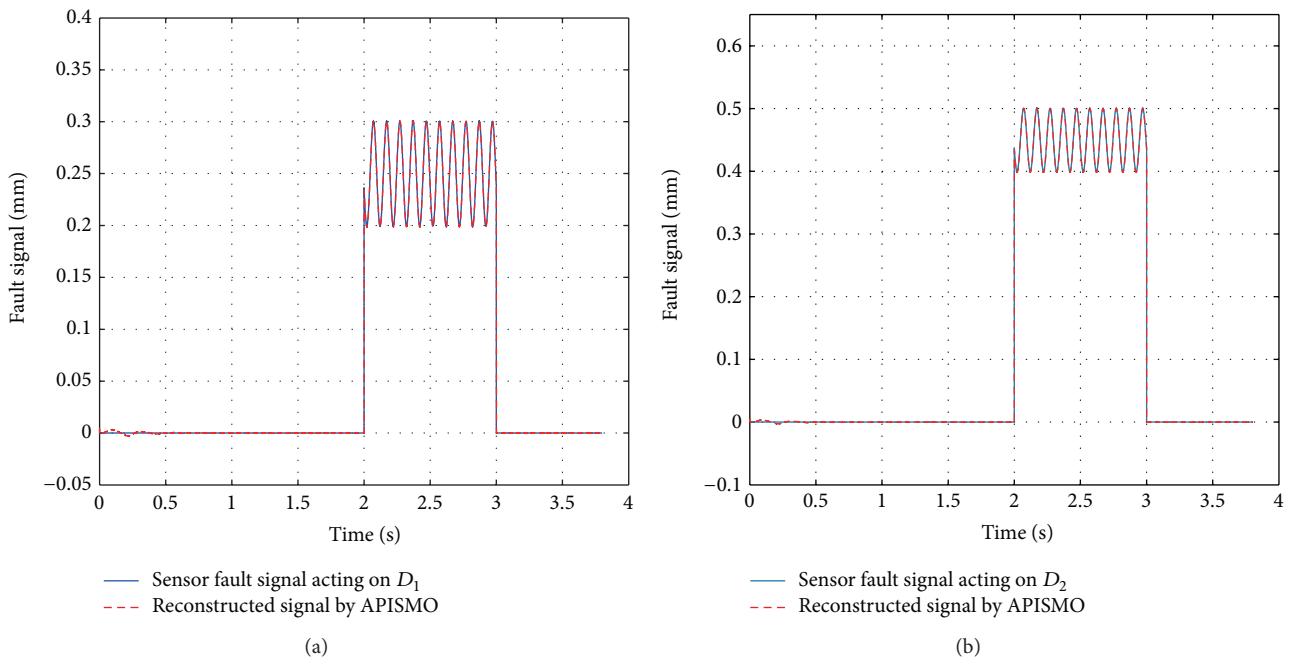


FIGURE 10: (a) Fault acting on sensor D_1 and its reconstruction by APISMO. (b) Fault acting on sensor D_2 and its reconstruction by APISMO.

shown in Figure 11(b), when the fault signal is larger than the scalar ρ , the conventional SMO cannot reconstruct the fault signal properly.

Figure 12 shows the positions measured by the two primary sensors and the estimated positions provided by APISMO when faults occur. It is observed that, in the presence of faults, the estimated outputs by APISMO are

maintaining the accurate values. Consequently, the performance of the control system could be kept approximately by the estimation during the backup booting up.

5.4. Fault-Tolerant Control Implementation. The performance of the proposed FTC scheme is verified by several experimental studies conducted hereinafter.

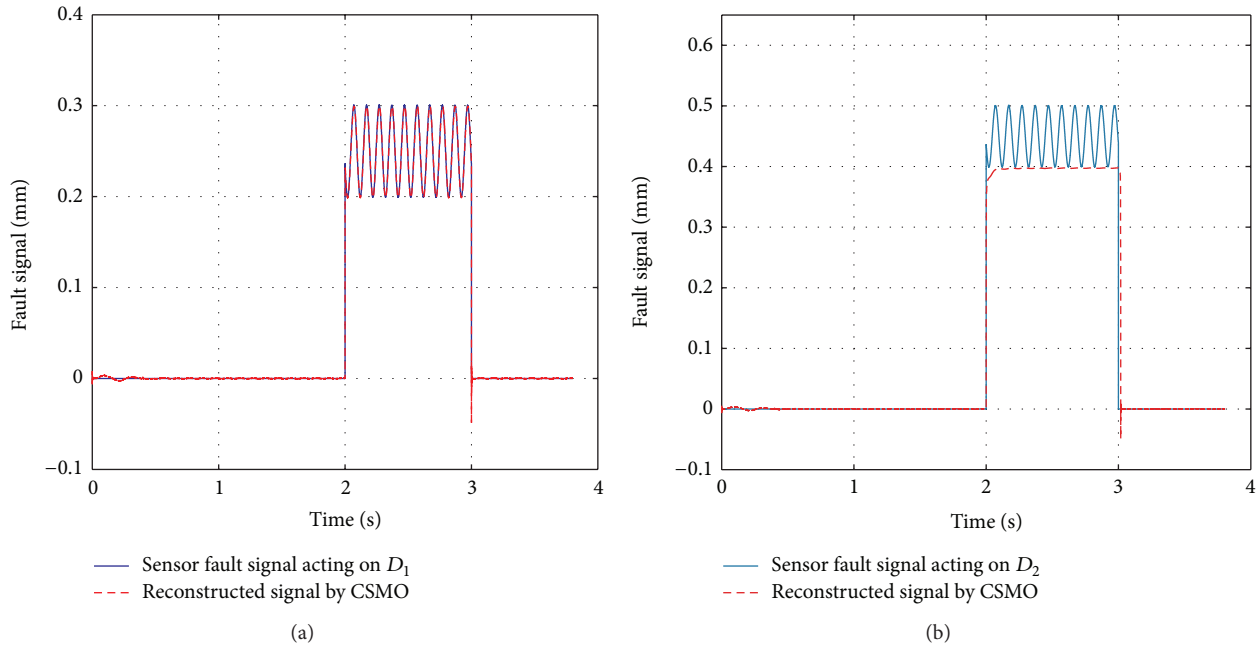


FIGURE 11: (a) Fault acting on sensor D_1 and its reconstruction by conventional SMO (CSMO). (b) Fault acting on sensor D_2 and its reconstruction by conventional SMO (CSMO).

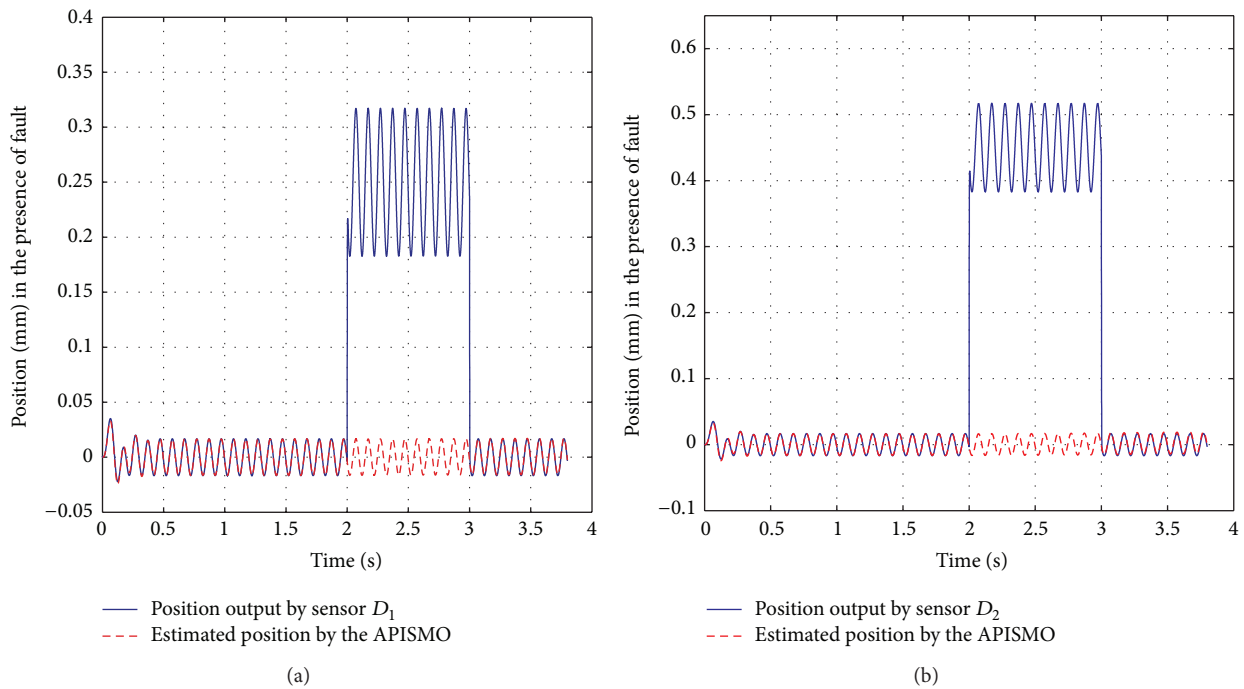


FIGURE 12: (a) Position measured by sensor D_1 and the position estimated by APISMO when fault occurs. (b) Position measured by sensor D_2 and the position estimated by APISMO when fault occurs.

Since the FSM was designed as a decoupled parallel-kinematic structure, for the purpose of validating the proposed FTC scheme, only one traditional PI controller has been designed to handle the mirror rotating about x -axis. The design parameter for fault isolation was chosen as $N = 10$ cycles of the counter, equaling 2 ms at 200 μ s sampling

time. This value represents a reasonable compromise between accuracy and short isolation time. The threshold was chosen as 0.1 V, that is, 5 μ m. The sensor fault acting on D_1 is shown in Figure 13(a). For the purpose of comparison, Figure 13(b) shows the position tracking error provided by the traditional PI controller in fault-free case. When fault in Figure 13(a) is

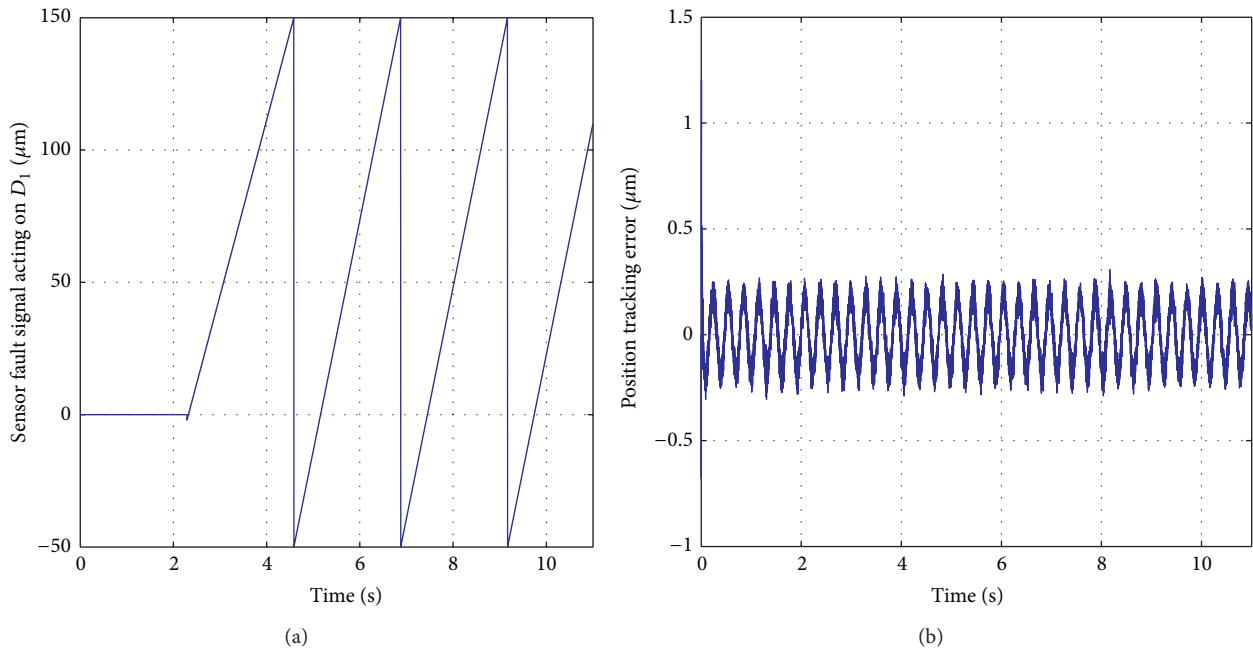


FIGURE 13: (a) Sensor fault signal acting on D_1 . (b) The position tracking error of the PI controller in fault-free case.

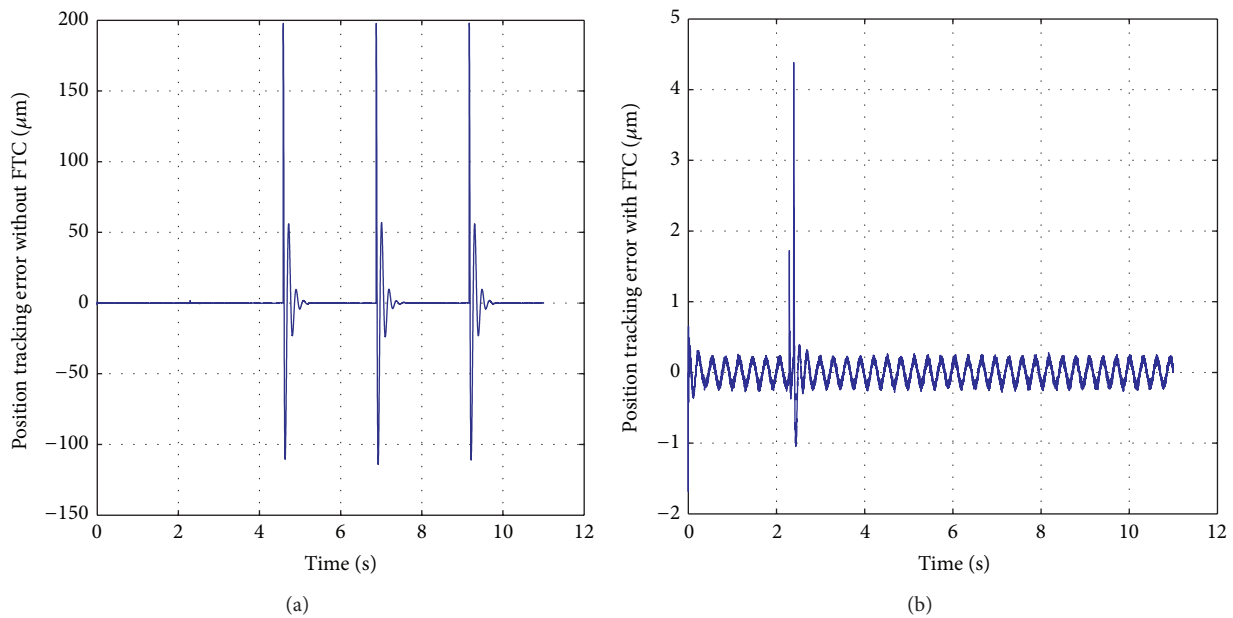


FIGURE 14: The position tracking error in the presence of fault (a) when the FTC scheme is not adopted, (b) when the FTC scheme is implemented.

acting on the primary sensor D_1 , the tracking error provided by the PI controller without the FTC scheme is shown in Figure 14(a). It is obvious that the tracking performance of the control system is degraded.

The proposed FTC scheme illustrated in Figure 4 has been implemented to maintain the desired performance in the presence of sensor fault. The position tracking error of the proposed FTC scheme is shown in Figure 14(b). As

seen in Figure 14(b), when the reconstructed fault signal has exceeded the threshold for about 2 ms, the fault would be detected and isolated by the logic, and the estimation of the position provided by the APISMO would be used by the controller. After the backup is activated, the measurement of the redundant sensor would be used as feedback signal. It can be seen that the proposed FTC scheme could maintain near to desired performance when fault occurs.

6. Conclusion

In this paper, a novel FTC scheme for the fast steering mirror system was proposed by integrating an adaptive PI-based sliding mode observer and hardware redundancy. The controller structure did not need to be changed. The proposed scheme adopted an APISMO to reconstruct the fault signal. The advantage of this method is that it does not require any prior knowledge of the faults and has no chattering. The reachability of the sliding surface has been examined. In order to keep the controller free from the sensor faults, fault isolation logic was used to identify the fault and power up the redundant sensor. During the cold backup booting up, the performance of the control system was maintained approximately by estimations of the position provided by the APISMO. Experiments have been conducted to verify the scheme. The experimental results confirmed that FSM system with the proposed FTC scheme could maintain a good tracking despite the presence of the fault.

Since the proposed FTC scheme is easy to be implemented and does not require any prior knowledge of the faults, it can be widely extended to other types of beam control systems. In the experiments, since only the position signal was measured, there was no freedom left to deal with the measurement noises and model uncertainties. Nevertheless, experimental results showed that the effect of the noises and uncertainties on the FTC was not significant. Future works will focus on dealing with measurement noises and model uncertainties.

Conflict of Interests

The authors declare that there is no conflict of interests regarding the publication of this paper.

Acknowledgment

This work was supported by Grant no. A09K002 from the Advanced Research Foundation of the Key Laboratory, Chinese Academy of Sciences.

References

- [1] R. Zhang, J. Wang, G. Zhao, and J. Lv, "Fiber-based free-space optical coherent receiver with vibration compensation mechanism," *Optics Express*, vol. 21, no. 15, pp. 18434–18441, 2013.
- [2] M. Ostaszewski and W. Vermeer, "Fine steering mirror for the James Webb Space Telescope," in *New Developments in Optomechanics*, vol. 6665, p. D6650, 2007.
- [3] A. Bullard and I. Shawki, "Responder fast steering mirror," in *Sensors, Systems, and Next-Generation Satellites XVII*, vol. 8889 of *Proceedings of SPIE*, 2013.
- [4] T. Tang, Y. Huang, C. Fu, and S. Liu, "Acceleration feedback of a CCD-based tracking loop for fast steering mirror," *Optical Engineering*, vol. 48, no. 1, Article ID 013001, 2009.
- [5] T. Tang, R. Ge, J. Ma, and C. Fu, "Compensating for some errors related to time delay in a charge-coupled-device-based fast steering mirror control system using a feedforward loop," *Optical Engineering*, vol. 49, no. 7, Article ID 073005, 2010.
- [6] X. Wu, S. Chen, B. Shi, W. Chen, and X. Xiong, "High-powered voice coil actuator for fast steering mirror," *Optical Engineering*, vol. 50, no. 2, Article ID 023002, 2011.
- [7] I. Pain, B. Stobie, G. S. Wright, T. A. Paul, and C. R. Cunningham, "The SPIRE beam steering mirror: a cryogenic 2 axis mechanism for the Herschel space observatory," in *IRSpace Telescopes and Instruments, Parts 1 and 2*, vol. 4850, pp. 619–627, 2003.
- [8] D. Gorinevsky, G. M. Hoffmann, M. Shmakova, R. W. Mah, S. Cryan, and J. D. Mitchell, "Fault tolerance of relative navigation sensing in Docking approach of spacecraft," in *Proceedings of the IEEE Aerospace Conference (AC '08)*, pp. 1–9, March 2008.
- [9] J. Blesa, D. Rotondo, V. Puig, and F. Nejari, "FDI and FTC of wind turbines using the interval observer approach and virtual actuators/sensors," *Control Engineering Practice*, vol. 24, no. 1, pp. 138–155, 2014.
- [10] B. Tabbache, M. E. H. Benbouzid, A. Kheloui, and J.-M. Bourgeot, "Virtual-sensor-based maximum-likelihood voting approach for fault-tolerant control of electric vehicle power-trains," *IEEE Transactions on Vehicular Technology*, vol. 62, no. 3, pp. 1075–1083, 2013.
- [11] J.-C. Ponsart, D. Theilliol, and C. Aubrun, "Virtual sensors design for active fault tolerant control system applied to a winding machine," *Control Engineering Practice*, vol. 18, no. 9, pp. 1037–1044, 2010.
- [12] S. Anwar and L. Chen, "An analytical redundancy-based fault detection and isolation algorithm for a road-wheel control subsystem in a steer-by-wire system," *IEEE Transactions on Vehicular Technology*, vol. 56, no. 5, pp. 2859–2869, 2007.
- [13] N. Venkateswaran, M. S. Siva, and P. S. Goel, "Analytical redundancy based fault detection of gyroscopes in spacecraft applications," *Acta Astronautica*, vol. 50, no. 9, pp. 535–545, 2002.
- [14] K. Zhang, B. Jiang, and P. Shi, "Observer-based integrated robust fault estimation and accommodation design for discrete-time systems," *International Journal of Control*, vol. 83, no. 6, pp. 1167–1181, 2010.
- [15] K. Zhang, B. Jiang, and P. Shi, "Fast fault estimation and accommodation for dynamical systems," *IET Control Theory & Applications*, vol. 3, no. 2, pp. 189–199, 2009.
- [16] K. Zhang, B. Jiang, and V. Cocquempot, "Adaptive observer-based fast fault estimation," *International Journal of Control, Automation and Systems*, vol. 6, no. 3, pp. 320–326, 2008.
- [17] H. Alwi and C. Edwards, "Fault detection and fault-tolerant control of a civil aircraft using a sliding-mode-based scheme," *IEEE Transactions on Control Systems Technology*, vol. 16, no. 3, pp. 499–510, 2008.
- [18] C. P. Tan and C. Edwards, "Sliding mode observers for robust detection and reconstruction of actuator and sensor faults," *International Journal of Robust and Nonlinear Control*, vol. 13, no. 5, pp. 443–463, 2003.
- [19] C. P. Tan and C. Edwards, "Sliding mode observers for detection and reconstruction of sensor faults," *Automatica*, vol. 38, no. 10, pp. 1815–1821, 2002.
- [20] C. Edwards, S. K. Spurgeon, and R. J. Patton, "Sliding mode observers for fault detection and isolation," *Automatica*, vol. 36, no. 4, pp. 541–553, 2000.
- [21] H. Alwi, C. Edwards, and C. P. Tan, "Sliding mode estimation schemes for incipient sensor faults," *Automatica*, vol. 45, no. 7, pp. 1679–1685, 2009.

- [22] C. Edwards and C. P. Tan, "Sensor fault tolerant control using sliding mode observers," *Control Engineering Practice*, vol. 14, no. 8, pp. 897–908, 2006.
- [23] A. Zolghadri, "Advanced model-based FDIR techniques for aerospace systems: today challenges and opportunities," *Progress in Aerospace Sciences*, vol. 53, pp. 18–29, 2012.
- [24] M. Z. Li, F. L. Wang, and F. R. Gao, "PID-based sliding mode controller for nonlinear processes," *Industrial and Engineering Chemistry Research*, vol. 40, no. 12, pp. 2660–2667, 2001.
- [25] J. Li and L. Yang, "Adaptive PI-based sliding mode control for nanopositioning of piezoelectric actuators," *Mathematical Problems in Engineering*, vol. 2014, Article ID 357864, 10 pages, 2014.
- [26] P. V. Mitchell, P. B. Griffith, and D. K. Henderson, "Fast-steering mirrors improve active beam stabilization," *Laser Focus World*, vol. 37, no. 10, pp. S13–S17, 2001.
- [27] Q. Zhou, P. Ben-Tzvi, D. Fan, and A. A. Goldenberg, "Design of fast steering mirror systems for precision laser beams steering," in *Proceedings of the International Workshop on Robotic and Sensors Environments*, pp. 144–149, Ottawa, Canada, April 1995.
- [28] Q. S. Xu and Y. M. Li, "Micro-/nanopositioning using model predictive output integral discrete sliding mode control," *IEEE Transactions on Industrial Electronics*, vol. 59, pp. 1161–1170, 2012.
- [29] C. Edwards and C. P. Tan, "A comparison of sliding mode and unknown input observers for fault reconstruction," *European Journal of Control*, vol. 12, no. 3, pp. 245–260, 2006.



Hindawi

Submit your manuscripts at
<http://www.hindawi.com>

